Chemical Science

ROYAL SOCIETY OF CHEMISTRY

EDGE ARTICLE

View Article Online
View Journal | View Issue

Cite this: *Chem. Sci.*, 2022, **13**, 14366

All publication charges for this article have been paid for by the Royal Society of Chemistry

Bidentate substrate binding in Brønsted acid catalysis: structural space, hydrogen bonding and dimerization†

Johannes Gramüller,[a] Philipp Dullinger,[b] Dominik Horinek[b] and Ruth M. Gschwind*[a]

Received 11th September 2022
Accepted 24th November 2022

DOI: 10.1039/d2sc05076e

rsc.li/chemical-science

BINOL derived chiral phosphoric acids (CPAs) are a prominent class of catalysts in the field of asymmetric organocatalysis, capable of transforming a wide selection of substrates with high stereoselectivities. Exploiting the Brønsted acidic and basic dual functionality of CPAs, substrates with both a hydrogen bond acceptor and donor functionality are frequently used as the resulting bidentate binding *via* two hydrogen bonds is expected to strongly confine the possible structural space and thus yield high stereoselectivities. Despite the huge success of CPAs and the popularity of a bidentate binding motif, experimental insights into their organization and origin of stereoinduction are scarce. Therefore, in this work the structural space and hydrogen bonding of CPAs and *N*-(*ortho*-hydroxyaryl) imines (19 CPA/imine combinations) was elucidated by low temperature NMR studies and corroborated by computations. The postulated bidentate binding of catalyst and substrate by two hydrogen bonds was experimentally validated by detection of *trans*-hydrogen bond scalar couplings. Counterintuitively, the resulting CPA/imine complexes showed a broad potential structural space and a strong preference towards the formation of $[CPA/imine]_2$ dimers. Molecular dynamics simulations showed that in these dimers, the imines form each one hydrogen bond to two CPA molecules, effectively bridging them. By finetuning steric repulsion and noncovalent interactions, rigid and well-defined CPA/imine monomers could be obtained. NOESY studies corroborated by theoretical calculations revealed the structure of that complex, in which the imine is located in between the 3,3′-substituents of the catalyst and one site of the substrate is shielded by the catalyst, pinpointing the origin or stereoselectivity for downstream transformations.

Introduction

Since their initial report by Akiyama[1] and Terada[2] in 2004, chiral Brønsted Acids have emerged as a powerful type of catalyst, adaptable to a myriad of asymmetric transformations.[3–5] The general concept is to lower the LUMO (Lowest Unoccupied Molecular Orbital) energy of the substrate *via* protonation by the Brønsted acidic catalyst functionality, thus facilitating a reaction with a nucleophile. By creating a stereoinductive environment around the substrate due to Coulomb-, hydrogen bonding- and other non-covalent interactions, the catalyst paves an asymmetric pathway for the reaction. The versatility of chiral Brønsted acids is augmented by a Brønsted basic site, which enables additional modes of activation and organization of the reactants (see Fig. 1 top).[5]

Exemplarily, the phosphoryl functionality of BINOL derived chiral phosphoric acids (CPA) can act as a hydrogen bond acceptor towards nucleophiles bearing a hydrogen bond donor, thus organizing both electro- and nucleophile in a defined way.[6–10] This "three-point-interaction model" was recognized to be crucial for delivering high stereoselectivities.[11–13] Moreover, by implementing both a hydrogen bond acceptor and donor functionality into the substrate,[14–21] bidentate binding of the catalyst and substrate results in a presumably rigid pre-organization of the substrate, in which one side of the substrate is shielded by the catalyst residues.

In their seminal report on CPA catalysed Mannich-type reactions, Akiyama *et al.* employed such a bidentate binding motif with the intention to furnish a highly confined structural space (see Fig. 1, right part) and noted a significant change in enantioselectivity, if the *ortho*-hydroxy group was omitted or placed in *para*-position.[14] Their computational study revealed a transition state, in which the substrate is anchored by two hydrogen bonds and is located in between the 3,3′-

[a]*Institut für Organische Chemie, Universität Regensburg, D-93053 Regensburg, Germany. E-mail: ruth.gschwind@chemie.uni-regensburg.de*

[b]*Institute of Physical and Theoretical Chemistry, University of Regensburg, D-93053, Germany*

† Electronic supplementary information (ESI) available. See DOI: https://doi.org/10.1039/d2sc05076e

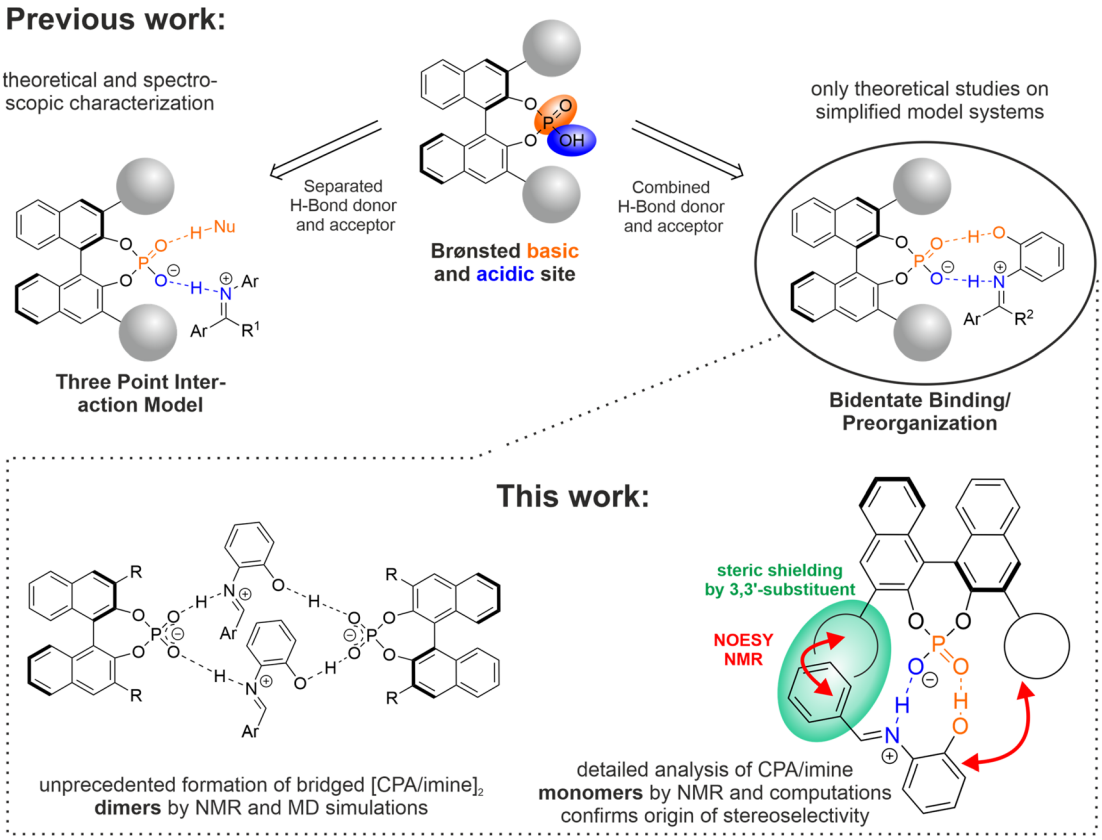

Fig. 1 (Top) Dual functionality of Brønsted acids enabling either parallel binding of electro- and nucleophile or bidentate binding of the substrate in a presumably rigid, defined way by hydrogen bonding. While the parallel binding motif is well explored experimentally and *in silico*, no detailed experimental insights exist for the bidentate binding motif. (Bottom) Key questions and results of the presented work feature spectroscopic and computational studies on the monomeric CPA/imine complex, confirming the surmised origin of stereoselectivity and unprecedented detection of $[CPA/imine]_2$ bridged dimers.

substituents.[14] This orientation is similar to the transition states which were found *e.g.* for the transfer hydrogenation of imines with Hantzsch ester[11,22] reflecting the "three-point-interaction model" and to dimers of complexes featuring CPAs and imines without additional hydrogen bond donors.[23] However, to the best of our knowledge experimental insights into the structural space of bidentate CPA/substrate complexes are limited to one recent example in asymmetric photocatalysis provided by our group, in which no detailed structural analysis could be derived.[19]

Therefore, in this report we present a detailed NMR spectroscopic study corroborated by molecular dynamics (MD) simulations on the structural space and hydrogen bonding of complexes featuring 8 CPAs and 8 *N*-(*ortho*-hydroxyaryl) imines (19 CPA/imine combinations). Low temperature NMR measurements revealed a broad structural space with a strong preference for the formation of $[CPA/imine]_2$ dimers, demonstrating that the principal idea of using a bidentate binding motif to restrict the structural space is not applying. MD simulations revealed that different dimer motifs are thermally accessible, in which each imine molecule bridges two different CPA molecules *via* hydrogen bonding. Breaking these dimers by fine-tuning steric repulsion and non-covalent interactions gave access to a rigid and well-defined monomeric CPA/imine complex. Combined NOESY NMR studies and computations revealed the structure of this monomeric complex and confirmed the assumed origin of stereoselectivity for downstream transformations.

Results and discussion

Initial system screening and dimer formation

To obtain an access to the structural space of bidentate CPA/imine complexes, an initial system screening with catalysts **1a–c** and imines **2a–c** was carried out (see Fig. 2A). Catalysts **1a–c** were selected due to their wide application in synthesis, their symmetry, solubility and different steric properties. For imines **2a–c**, a *para*-methoxy residue was selected as potential probe for structural investigations *via* NOESY NMR and the α-imine substituent was varied to modulate steric effects and subsequently the ratio between *E* and *Z* imine (*Z* population increasing for α-H < α-CH_3 < α-Ph). All NMR measurements were carried out at a temperature of 180 K to slow down potential exchange processes and thus to obtain an optimally resolved hydrogen bond pattern. In the previous work by Akiyama,[1,14] toluene was used as solvent as it yielded the best

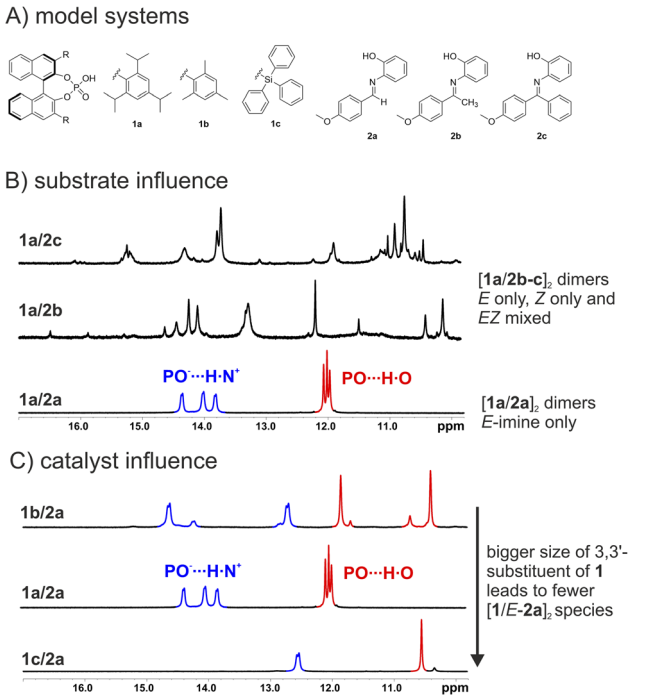

Fig. 2 (A) Selected catalysts and substrates for the initial system screening. (B) Section of the ^{1}H NMR spectra of **1a**/**2a** (bottom), **1a**/**2b** (middle) and **1a**/**2c** (top) at a 1 : 1 ratio and a concentration of 50, 10 and 10 mM respectively in CD_2Cl_2 at 600 MHz and 180 K. For **1a**/**2a**, three distinct species were observed, while for **1a**/**2b–c**, a multitude of different signals was monitored. (C) Section of the ^{1}H NMR spectra of **1a**/**2a** (middle), **1b**/**2a** (top) and **1c**/**2a** (bottom) at a 1 : 1 ratio and a concentration of 50, 10 and 10 mM respectively in CD_2Cl_2 at 600 MHz and 180 K.

stereoselectivity in the initial reaction optimization. However, similar to our previous studies,[24] the low temperature ^{1}H-NMR spectra in toluene gave very broad signals and were not suitable for further investigations (see ESI Fig. S4†). Hence dichloromethane (CD_2Cl_2) was selected as solvent for the NMR investigations, providing superior signal dispersion, linewidths and solubility. In addition, previous studies of CPA/imine complexes were successfully conducted in CD_2Cl_2 in our working group.[23–26]

For the system **1a**/**2a**, 6 proton signals were monitored in the H-bond region of the spectrum, corresponding to 3 distinct CPA/imine complexes with a ratio of ~1 : 1.7 : 1.1. The signals at ~14 ppm (Fig. 2B, blue signals) were assigned to the PO$^-$···H–N$^+$ hydrogen bonds based on the scalar coupling to the α-H protons of **2a** ($^{2h}J_{HH}$ = 13.6 Hz), which was confirmed by ^{1}H ^{1}H COSY spectrum. The signals at ~12 ppm (Fig. 2B, red signals) reflect the PO···H–O hydrogen bonds and were assigned based on cross signals in the ^{1}H ^{31}P HMBC spectrum and cross peaks with the protons of the *N*-aryl group in the ^{1}H ^{1}H COSY spectrum.

In contrast, for **1a**/**2b–c** (see Fig. 2B) a multitude of hydrogen bonded proton signals is detected, reflecting an unexpected broad structural space (similar spectra were obtained for **1b**/**2b–c**; see ESI S6†). For **1a**/**2a**, the three observed species could be assigned as different [**1a**/*E*-**2a**]$_2$ dimers, featuring exclusively the *E*-imine (see below). For **1a–b**/**2b–c**, we strongly assume that analogous [CPA/imine]$_2$ dimers are present, featuring either the *E*- or *Z*-imine or a mixture of both which increases the number of observed species. This variety of dimeric structures in combination with the potential presence of additional monomeric [CPA/imine] species causes the observed broad structural space reflected in the multitude of different H-bonded proton signals.

To obtain more detailed structural insights, in the following the system **1a**/**2a** was investigated. Low temperature sample preparation and photo-isomerization experiments (see ESI Fig. S7 and S8† for detailed discussion) validated that all 3 species exclusively feature *E*-imines. This is in agreement with previous findings that the size of the α-substituent is one major driving force towards the *Z*-imine besides reduced steric hindrance within the CPA binding pocket.[23,24] Based on a series of two-dimensional NMR spectra, a partial chemical shift analysis could be achieved for the three **1a**/**2a** species (see ESI Fig. S1†), however detailed structural insights *via* analysis of the NOESY spectrum could not be obtained due to line broadening and severe signal overlap. To shed light onto the nature of the **1a**/**2a** complexes, Diffusion Ordered Spectroscopy (DOSY) NMR measurements were carried out. For all three species, similar self-diffusion coefficients were found and an average hydrodynamic radius of 11.8 ± 0.87 Å was derived, which is similar to the previously reported radius of [**1b**/imine]$_2$ dimers.[23] A control experiment with catalyst **1a** and a reference imine without *ortho*-hydroxy group (see ESI Tables S1 and S2† for further details) gave a hydrodynamic radius of 8.8 ± 0.15 Å, which matches the previously reported radii for monomeric CPA/imine complexes.[23] Hence, for **1a**/**2a**, three [CPA/*E*-imine]$_2$ dimers with different hydrogen bonding situations are formed (see below for further discussion). For substrate **2a**, the selected CPA had a strong effect on the number of observed hydrogen bonded proton signals and thus number of species present (see Fig. 2C). While for catalyst **1a** three different species were monitored, four species were observed for **1b** and only one species for catalyst **1c**. For **1c**/**2a**, no further detailed NMR-spectroscopic studies were performed due to strong signal overlap in the aromatic region. However, DOSY measurements revealed a hydrodynamic radius of ~12.4 Å, clearly indicating it as a dimeric species (see ESI Table S5†). Based on the similar signal pattern and chemical shift range, we assume that the 4 different species observed for **1b**/**2a** are also dimers. Noteworthy, for the selected set of catalysts **1a–c**/**2a**, the size of the 3,3′-substituents (**1c** > **1a** > **1b**)[27] correlates with the number of observed species (**1c** < **1a** < **1b**), hinting that bulkier catalyst residues can restrict the structural space of the dimeric [CPA/imine]$_2$ species.

Molecular dynamic simulations of [1a/2a]$_2$ dimers

As a detailed structural analysis by NMR spectroscopy for **1a**/**2a** was not fruitful due to signal overlap and line broadening, simulations were performed to shed light onto the general differences between the at least three observed dimeric species. Hence, force field MD simulations at conditions similar to the

NMR experiments (1 bar, 200 K, $c = 50$ mM in CH_2Cl_2 – details see ESI†) were performed. Force field MD is the method of choice for investigating dynamic, aggregation and H-bonding behaviour of the molecules **1a**/**2a** in solution at finite temperature with reasonable computational cost. Since the NMR experiments show that the molecules are hydrogen bond assisted ion pairs (see ESI chapter 7 for further discussion†) exclusively the ion pair protonation state (phosphate and iminium) were simulated. Thus, dissociation is unfavourable and was not observed in the simulations. In our previous research on imine substrates without an *ortho*-hydroxy substituent, we detected and characterized dimeric $[CPA/imine]_2$ complexes, in which the two imines were stacked in a shifted face-to-face arrangement between two CPA molecules.[23] However, for the *ortho*-hydroxy substituted imines, in principle two general hydrogen bonding arrangements can be envisioned: either one imine is bound to one CPA *via* a bidentate binding motif (as shown in Fig. 1 top right) and two of these units aggregate (non-bridging H-bond motif) or each imine molecule bridges two different CPA molecules *via* hydrogen bonding (bridging H-bond motif; see Fig. 3).

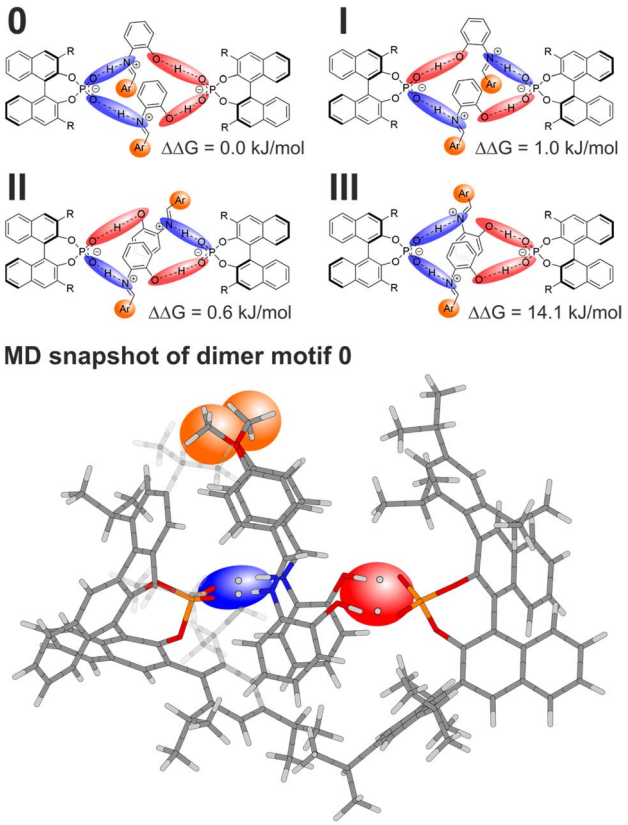

Fig. 3 (Top) Sketch of the four different bridging H-bond dimer motifs 0–III investigated in the MD simulations for **1a**/**2a**, featuring two CPA and two imine molecules. In all motifs, two different CPA molecules are bridged by two imines *via* hydrogen bonding. Both $PO^-\cdots H-N^+$ hydrogen bonds (blue) can point towards one CPA, while the two $PO\cdots H\cdots O$ hydrogen bonds (red) are directed to the other CPA (motifs 0 and III) or each CPA can form one $PO^-\cdots H-N^+$ and one $PO\cdots H\cdots O$ hydrogen bond (motifs I and II). The imine can be stacked parallel (motifs 0 and I) or antiparallel (motifs II and III). (Bottom) MD snapshot for dimer motif 0, highlighting the bridging of two CPA molecules by two imines. Colour code: red: oxygen; blue: nitrogen; dark grey: carbon; light grey: hydrogen.

A cluster analysis for an initial simulation with individual CPA and iminium molecules of **1a**/**2a** showed no significant number of non-bridging dimers. This strongly indicates that the bridging motif (one imine binds to two CPAs) is favored over the bidentate binding. For the bridged dimers, four different arrangements are generally possible. In all cases two CPA molecules are interconnected by four hydrogen bonds over two imine molecules nested in between the CPAs (see Fig. 3 top). Their differences originate in the orientation of the second imine molecule. Both $PO^-\cdots H-N^+$ hydrogen bonds can be directed to one CPA, while both $PO\cdots H\cdots O$ hydrogen bonds point to the second CPA molecule (dimer 0 and III) or each CPA forms one $PO^-\cdots H-N^+$ and one $PO\cdots H\cdots O$ hydrogen bond (I and II). In addition, the second imine can be orientated parallel (0 and I) or antiparallel (II and III). Thermodynamic integration free energy simulations revealed that motifs 0, I and II are similarly thermally accessible, while motif III is 13–14 kJ mol^{-1} higher in free energy and thermally not accessible (see ESI Table S8†). While in dimers 0–II the two imines are stacked in a shifted face-to-face arrangement (see Fig. 3 bottom), this is not the case for motif III (compared to the other motif 0 with similar hydrogen bond orientation, the interaction is much weaker). Thus, we assume that the three dimer species observed in the ^{1}H NMR spectrum for **1a**/**2a** (see Fig. 2B) correspond to dimer motifs 0, I and II. Additionally, the MD simulations of motif 0 suggest that even for one specific bridging motif a high degree of flexibility exists, so that transitions between different conformations arising from a rotation of the BINOL backbone (on the side given by the iminium OH groups) of one CPA occur on a timescale below 100 ns (see ESI Fig. S19†). We explain the presence of two different conformations by a shift in van der Waals stabilisation from imine–imine to imine–CPA.

In our previous studies with imines without *ortho*-hydroxy substituents (only one hydrogen bond between CPA and imine), we identified $[CPA/imine]_2$ dimer complexes, in which two stacked imines are nested in between two CPA molecules. These dimers are proposed not to play a role in catalysis and resemble an off-cycle equilibrium with the catalytic relevant monomeric CPA/imine complexes, especially as additional binding of a nucleophile by a second hydrogen bond (see Fig. 1, left) is assumed to prevent formation of these dimers.[23] However, it was also shown that CPA molecules can form $PO\cdots H\cdots OP$ hydrogen bond bridged dimers which then can act as an alternative active catalyst, opening a concentration dependent dimeric reaction channel.[26] For CPA catalysed transformations of imines bearing an *ortho*-hydroxy substituent, originally a bidentate binding to the catalyst was proposed.[1] Typical third reaction partners[1,15,16,20] for imines with *ortho*-hydroxy substituent feature no hydrogen bond donor. Thus, only a weak pre-organisation can be envisioned within the CPA/imine/nucleophile complex. However, these transformations could in principle also proceed over the observed dimer motifs, in which the imine bridges two CPA molecules. This leads to a broad variety of potential transition states, featuring distinct

dimer motifs combined with different attack pathways for the nucleophile and potentially also contributions of the respective monomeric reaction pathways. However, the potential dimeric pathway implies that an application of catalyst mixtures (*e.g. R* and *S* enantiomers or two catalysts with different 3,3′-substituents) might prove beneficial for optimizing stereoselectivities.

After exploring the structural space of $[\mathbf{1a}/\mathbf{2a}]_2$ bridged dimers in solution by NMR and MD simulations, we focused on *para*-nitrophenyl substituted catalyst **1e** (see Fig. 4a), which showed the highest stereoselectivities in the initial report on CPA catalyzed Mannich reaction of aldimines by Akiyama.[1] Detailed NMR spectroscopic studies at low temperature were not possible due to the limited solubility of **1e** in CD_2Cl_2 at −93 °C (see ESI Fig. S9†). Therefore, MD simulations were performed, which suggest that the relative energy differences between the analogous $[\mathbf{1e}/\mathbf{2a}]_2$ dimer motifs are significantly stronger as for $[\mathbf{1a}/\mathbf{2a}]_2$, indicating a higher structural preference (see ESI Table S9†). However, in agreement with the low solubility of **1e** especially at low temperatures (the reaction was performed at −78 °C), mainly monomeric **1e**/**2a** complexes were observed in the simulations, despite intermediate appearance of additional hydrogen-bonded species (see ESI S25†). This might explain why nitro-substituted catalyst **1e** (and in a later study by Yamamoto *et al.* a 2,4,6-trimethyl-3,5-dinitrophenyl substituted CPA)[17] yielded the highest enantioselectivities, assuming that the structural space and solubility is not significantly different in dichloromethane and toluene. The broad structural space of the reaction intermediates, linked to a broad variety of potential transition states is reduced to the mainly monomeric pathway by the limited solubility of the catalyst.

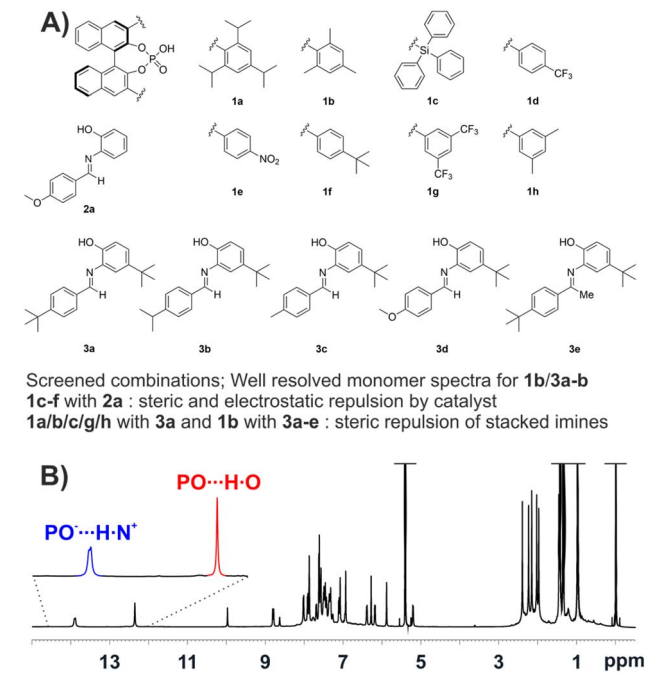

Fig. 4 (A) CPAs and imines which were tested in order to suppress dimer formation. CPAs **1c–f** were employed with substrate **2a** but no well resolved CPA/imine monomers were obtained (see ESI Fig. S9† for spectra and discussion). For imines **3a–e** well resolved CPA/imine monomers were only found for **1b**/**3a** and **1b**/**3b** (see ESI Fig. S10 and S11† for spectra and discussion). (B) ^{1}H NMR spectrum of **1b**/**3a** at a 1 : 1 ratio and a concentration of 25 mM at 180 K and 600 MHz in CD_2Cl_2 showing two hydrogen bonded proton signals respecting one single complex.

Accessing CPA/imine monomers

The strong tendency of **1**/**2** complexes towards dimerization opens up a multitude of different potential transition states. Thus, we were intrigued to study, which molecular features suppress dimer formation and force the system towards CPA/imine monomers for an easier selection of optimal catalysts. Since the MD simulations showed stacking of the imines in between the catalysts for all accessible dimers (see Fig. 3 bottom), we aimed to hinder dimerization by introducing electronic or steric repulsion.

After screening of 13 CPA/imine combinations (**1c–f**/**2a**; **1a–c**, **g**, **h**/**3a**; **1b**/**3a–e**; see Fig. 4A for selected CPAs and imines and ESI Fig. S9–S11† for respective ^{1}H NMR spectra and further discussion) we were able to obtain the well resolved system **1b**/**3a**, showing only two proton signals in the hydrogen bond region of the ^{1}H NMR spectrum (see Fig. 4B). DOSY measurements gave a hydrodynamic radius of 10.9 ± 0.15 Å for **1b**/**3a** and a value of 10.2 ± 0.16 Å was determined for a monomeric reference system (see ESI Tables S3 and S4†), clearly demonstrating that the observed species is a monomer. Using a combination of ^{1}H ^{1}H COSY, ^{1}H NOESY, ^{1}H ^{13}C HSQC, ^{1}H ^{13}C HMBC and ^{1}H ^{31}P HMBC spectra allowed for a complete chemical shift assignment of the complex (see ESI Fig. S2†). The proton signals at 13.91 ppm (Fig. 4B, blue signal) and 12.37 ppm (Fig. 4B, red signal) could unambiguously be characterized as the PO$^-$···H–N$^+$ and PO···H–O hydrogen bonded proton respectively by detection of *trans*-hydrogen bond scalar coupling *via* ^{1}H ^{1}H COSY and ^{1}H ^{31}P HMBC spectra (see ESI Fig. S12† for spectra and further discussion). In comparison to our previously investigated monodentate **1b**/imine systems,[28] the PO$^-$···H–N$^+$ hydrogen bond proton signal of **1b**/**3a** is significantly highfield shifted (∼2 ppm), which correlates to a weaker H-bond and a stronger proton transfer onto the substrate caused by the cooperativity effect of the second PO···H–O hydrogen bond.[26]

To shed light onto the structure of **1b**/**3a** in solution, an analysis of the NOE pattern was done and corroborated by calculations. Hence, **1b**/**3a** was optimized in CH_2Cl_2 (SMD) at the DFT level of theory employing Grimme's D3 empirical dispersion correction (TPSS-D3/dev2-SVP; see ESI for details†). The resulting most stable complex (see Fig. 5) was found to be analogous to the previously reported simplified structure model for CPAs and *N*-(*ortho*-hydroxyaryl) imines by Akiyama.[14]

In this complex, the imine is located in between the two 3,3′-substituents of the catalyst and anchored by two hydrogen bonds (see Fig. 5, blue area). One side of the substrate is sterically shielded by the 3,3′-substituent, effectively blocking this side for nucleophilic attacks. The computed structure model agrees with the performed NOESY NMR studies, which revealed contacts between the *N*-aryl moiety of the imine and one 3,3′-

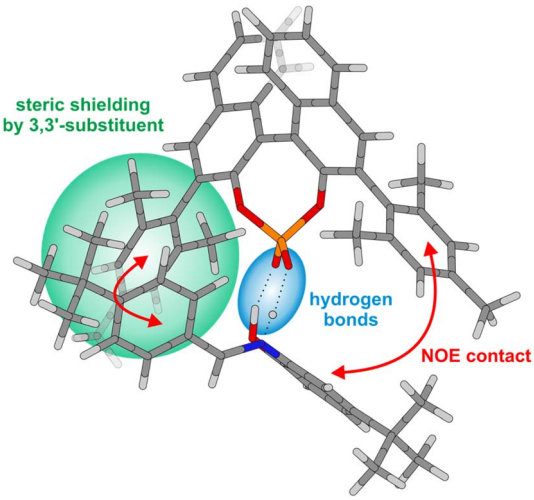

Fig. 5 DFT structure model of **1b**/**3a**. The two hydrogen bonds (highlighted in blue) anchor the substrate in between the two 3,3′-substituents of the catalyst. One side of the substrate is effectively shielded by the 3,3′-substituent, which causes the stereoinduction.

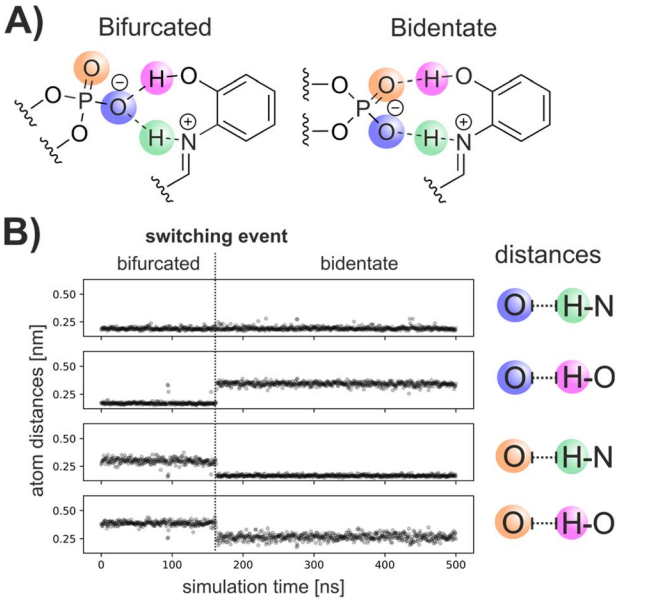

Fig. 6 (A) Bidentate and bifurcated hydrogen bonding motives. (B) Plot of atom distances of the Brønsted acidic and basic oxygen atom (blue and orange) and hydrogen bond protons (green and magenta) during the MD simulations reveals the rare switching event (dashed line) between two different binding motifs.

substituent of the CPA as well as between the *para*-^{t}butyl phenyl entity of the imine and the other 3,3′-substituent (Fig. 5, indicated by red arrows; see ESI Fig. S13† for NOESY spectrum). Additionally, no NOE contacts have been detected between the imine and the BINOL backbone as it is the case for the respective CPA/imine systems featuring only one hydrogen bond.[23,24] Remarkably, the two halves of the BINOL backbone, the two 3,3′-substituents and especially the two *ortho* as well as *para* protons of the *para*-^{t}butyl phenyl entity of the imine possess different chemical shifts. Signal splitting of the *ortho* and *para* protons clearly shows that rotation of the *para*-^{t}butyl phenyl ring is slow on the NMR timescale, which is in stark contrast to our previous investigations on CPA/imine systems with one hydrogen bond where such splitting was never monitored.[23,24] The observation that even the rotation of the phenyl group is hindered clearly indicates that the bidentate binding by two hydrogen bonds enforces a rigid and well defined preorganization of catalyst and imine. This is further corroborated by the signal splitting of the CPA, which was not present in our previous studies for many CPA/imine systems with one hydrogen bond due to signal averaging by fast interconversion of different conformers.[23,29]

Additionally, in the molecular dynamic simulations for monomeric aggregates of **1a**/**2a**, two different hydrogen bonding motifs were found. One features a bidentate binding of the imine towards both oxygen atoms of **1a**, while the other shows bifurcated binding towards only one oxygen atom (see Fig. 6A).

The two binding motifs can interconvert (rare event on the 100 ns timescale), indicating an equilibrium between these two binding states (the switching process occurs in both directions and thus is no equilibration artefact; see ESI Fig. S15–S17†). This hints that the Brønsted basic site of the CPA (see Fig. 1) might not be blocked entirely by the bidentate binding of a substrate featuring both a hydrogen bond donor and acceptor. Thus, for monomeric CPA/**2** complexes, a bifurcated binding of the imine substrate and additional binding of a nucleophile with H-bond donor (see Fig. 1 left) could be surmised for certain catalyst/substrate/nucleophile combinations.

Noteworthy, only the combination of **1b**/**3a** and **1b**/**3b** (see ESI Fig. S11†) gave a well resolved NMR spectrum of the monomer complex. Slight changes in the catalyst or the substrate led to a variety of species or dimerization of CPA and imine (see ESI Fig. S9–S11† for full overview of systems, spectra, and detailed discussion), indicating a broad structural space featuring different dimeric $[CPA/imine]_2$ complexes, hydrogen binding motifs and potentially other monomeric CPA/imine conformers. This is surprising, as a bidentate binding motif was expected to confine the structural space and minimize the number and variety of potential species. However, it remains elusive if and how this structural diversity might affect the catalysis or reflects off-cycle equilibriums.

Conclusion

A selection of BINOL derived chiral phosphoric acid catalysts and *N*-(*ortho*-hydroxyaryl) imines (19 CPA/imine combinations) was studied *via* NMR spectroscopy to shed light onto the structural space and hydrogen bonding of the respective CPA/imine complexes and to pinpoint the origin of stereoselectivity for related transformations of the imine substrates. Introducing an additional hydrogen bond donor into the substrate (*ortho*-hydroxy group) led to bidentate binding of catalyst and substrate *via* the formation of two hydrogen bonds. The resulting CPA/imine complexes showed a broad structural space with a variety of different species and a preference for the

formation of $[CPA/imine]_2$ dimers, contradicting the general assumption, that bidentate binding of CPA and substrate results in a highly confined structural space, thus yielding high enantioselectivities. MD simulations showed, that in these dimers, the imines may form each one hydrogen bond to two CPA molecules, effectively bridging them. This indicates that respective transformation might proceed *via* $[CPA/imine]_2$ dimers instead of bidentate bound CPA/imine complexes, implying that catalyst mixtures (either *R* and *S* enantiomer or two catalysts with different 3,3′-substituents) might prove beneficial for optimizing stereoselectivities. Modulating steric repulsion and noncovalent interactions allowed to access rigid and well-defined monomer structures. NOESY NMR studies corroborated by theoretical calculations showed, that the imine is located in between the two 3,3′-substituents of the catalyst. One side of the substrate is thereby shielded by the catalyst, which creates the stereoinductive environment for asymmetric downstream transformations.

Data availability

Necessary data is given in the ESI.†

Author contributions

J. G. and R. G. conceived and conceptualised the project. J. G. planned and performed all experiments. Analysis of all experiments was done by J. G. and R. G. All calculations were performed by P. D. and analysed by P. D. and D. H. Visualisation was done by J. G. and P. D., interpretation of results, writing and revision of the manuscript was done by all authors. R. G. and D. H. provided funding and resources.

Conflicts of interest

There are no conflicts to declare.

Acknowledgements

We thank the German Science Foundation (DFG; SPP 1807 London Dispersion project number 397981750 and RTG 2620 project number 426795949) for financial and intellectual support. J. G. thanks the Fonds der chemischen Industrie for funding (Kekulé fellowship). P. D. thanks the Studienstiftung des deutschen Volkes for funding.

Notes and references

1 T. Akiyama, J. Itoh, K. Yokota and K. Fuchibe, *Angew. Chem., Int. Ed.*, 2004, **43**, 1566–1568.
2 D. Uraguchi and M. Terada, *J. Am. Chem. Soc.*, 2004, **126**, 5356–5357.
3 D. Parmar, E. Sugiono, S. Raja and M. Rueping, *Chem. Rev.*, 2014, **114**, 9047–9153.
4 T. Akiyama, *Chem. Rev.*, 2007, **107**, 5744–5758.
5 M. Terada, *Synthesis*, 2010, 1929–1982.
6 R. I. Storer, D. E. Carrera, Y. Ni and D. W. C. MacMillan, *J. Am. Chem. Soc.*, 2006, **128**, 84–86.
7 M. Rueping, E. Sugiono and C. Azap, *Angew. Chem., Int. Ed.*, 2006, **45**, 2617–2619.
8 Q. Kang, Z. A. Zhao and S. L. You, *J. Am. Chem. Soc.*, 2007, **129**, 1484–1485.
9 C. Zhu and T. Akiyama, *Org. Lett.*, 2009, **11**, 4180–4183.
10 X. Cheng, R. Goddard, G. Buth and B. List, *Angew. Chem., Int. Ed.*, 2008, **47**, 5079–5081.
11 L. Simón and J. M. Goodman, *J. Am. Chem. Soc.*, 2008, **130**, 8741–8747.
12 L. Simón and J. M. Goodman, *J. Am. Chem. Soc.*, 2009, **131**, 4070–4077.
13 L. Simón and J. M. Goodman, *J. Org. Chem.*, 2010, **75**, 589–597.
14 M. Yamanaka, J. Itoh, K. Fuchibe and T. Akiyama, *J. Am. Chem. Soc.*, 2007, **129**, 6756–6764.
15 T. Akiyama, H. Morita and K. Fuchibe, *J. Am. Chem. Soc.*, 2006, **128**, 13070–13071.
16 T. Akiyama, Y. Honma, J. Itoh and K. Fuchibe, *Adv. Synth. Catal.*, 2008, **350**, 399–402.
17 F. Zhou and H. Yamamoto, *Angew. Chem., Int. Ed.*, 2016, **55**, 8970–8974.
18 F. Pecho, Y. Q. Zou, J. Gramüller, T. Mori, S. M. Huber, A. Bauer, R. M. Gschwind and T. Bach, *Chem. - Eur. J.*, 2020, **26**, 5190–5194.
19 F. Pecho, Y. Sempere, J. Gramüller, F. M. Hörmann, R. M. Gschwind and T. Bach, *J. Am. Chem. Soc.*, 2021, **143**, 9350–9354.
20 T. Akiyama, Y. Tamura, J. Itoh, H. Morita and K. Fuchibe, *Synlett*, 2006, 141–143.
21 J. Itoh, K. Fuchibe and T. Akiyama, *Angew. Chem., Int. Ed.*, 2006, **45**, 4796–4798.
22 T. Marcelli, P. Hammar and F. Himo, *Chem. - Eur. J.*, 2008, **14**, 8562–8571.
23 M. Melikian, J. Gramüller, J. Hioe, J. Greindl and R. M. Gschwind, *Chem. Sci.*, 2019, **10**, 5226–5234.
24 J. Greindl, J. Hioe, N. Sorgenfrei, F. D. Morana and R. M. Gschwind, *J. Am. Chem. Soc.*, 2016, **138**, 15965–15971.
25 N. Sorgenfrei, J. Hioe, J. Greindl, K. Rothermel, F. Morana, N. Lokesh and R. M. Gschwind, *J. Am. Chem. Soc.*, 2016, **138**, 16345–16354.
26 D. Jansen, J. Gramüller, F. Niemeyer, T. Schaller, M. C. Letzel, S. Grimme, H. Zhu, R. M. Gschwind and J. Niemeyer, *Chem. Sci.*, 2020, **11**, 4381–4390.
27 J. P. Reid and J. M. Goodman, *J. Am. Chem. Soc.*, 2016, **138**, 7910–7917.
28 K. Rothermel, M. Melikian, J. Hioe, J. Greindl, J. Gramüller, M. Žabka, N. Sorgenfrei, T. Hausler, F. Morana and R. M. Gschwind, *Chem. Sci.*, 2019, **10**, 10025–10034.
29 N. Lokesh, J. Hioe, J. Gramüller and R. M. Gschwind, *J. Am. Chem. Soc.*, 2019, **141**, 16398–16407.